Comparison of virtual unenhanced CT images of the abdomen under different iodine flow rates

Yongrui Li,[1] Ye Li,[1] Alan Jackson,[2] Xiaodong Li,[1] Ning Huang,[3] Chunjie Guo,[1] Huimao Zhang[1]

[1]Department of Radiology, The First Hospital of JiLin University, Changchun 130000, Jilin, China
[2]Wolfson Molecular Imaging Center, University of Manchester, Withington, Manchester M20 3LJ, UK
[3]GE Healthcare (Life Science), Beijing 100176, China

Abstract

Objective: To assess the effect of varying iodine flow rate (IFR) and iodine concentration on the quality of virtual unenhanced (VUE) images of the abdomen obtained with dual-energy CT.
Methods: 94 subjects underwent unenhanced and triphasic contrast-enhanced CT scan of the abdomen, including arterial phase, portal venous phase, and delayed phase using dual-energy CT. Patients were randomized into 4 groups with different IFRs or iodine concentrations. VUE images were generated at 70 keV. The CT values, image noise, SNR and CNR of aorta, portal vein, liver, liver lesion, pancreatic parenchyma, spleen, erector spinae, and retroperitoneal fat were recorded. Dose–length product and effective dose for an examination with and without plain phase scan were calculated to assess the potential dose savings. Two radiologists independently assessed subjective image quality using a five-point scale. The Kolmogorov–Smirnov test was used first to test for normal distribution. Where data conformed to a normal distribution, analysis of variance was used to compare mean HU values, image noise, SNRs and CNRs for the 4 image sets. Where data distribution was not normal, a nonparametric test (Kruskal–Wallis test followed by stepwise step-down comparisons) was used. The significance level for all tests was 0.01 (two-sided) to allow for type 2 errors due to multiple testing.
Results: The CT numbers (HU) of VUE images showed no significant differences between the 4 groups ($p > 0.05$) or between different phases within the same group ($p > 0.05$). VUE images had equal or higher SNR and CNR than true unenhanced images. VUE images received equal or lower subjective image quality scores than unenhanced images but were of acceptable quality for diagnostic use. Calculated dose–length product and estimated dose showed that the use of VUE images in place of unenhanced images would be associated with a dose saving of 25%.
Conclusions: VUE images can replace conventional unenhanced images. VUE images are not affected by varying iodine flow rates and iodine concentrations, and diagnostic examinations could be acquired with a potential dose saving of 25%.

Abbreviations

IFR	Iodine flow rate
VUE	Virtual unenhanced
AP	Arterial phase
VP	Portal venous phase
DP	Delayed phase
TUE	True unenhanced
DLP	Dose–length product
ED	Effective dose

Computed tomography (CT) is associated with radiation dosage. The introduction of new, higher dose CT imaging paradigms (compared with planar X-ray imaging techniques) such as multiphase and dynamic contrast-enhanced techniques, together with increased coverage and spatial resolution of modern systems, has led to prioritization of methods for radiation dose reduction. Modification of acquisition parameters [1, 2] can produce significant radiation savings as can under-sampling

Correspondence to: Huimao Zhang; *email:* huimaozhanglinda@163.com

combined with iterative reconstruction. The introduction of dual-energy CT, where two datasets are acquired at different energies, offers an opportunity for radiation dose reduction. Soft tissue attenuation is relatively unaffected by beam energy, but the attenuation of high-atomic number materials, such as iodine, is highly energy dependent. This allows the production of virtual monochromatic images (VMIs) that simulate the appearances which would have been expected with a monochromatic X-ray beam. In addition, iodine-related attenuation can be separated from tissue-related attenuation with the generation of an ''iodine map,'' allowing the production of virtual unenhanced (VUE) images from virtual monochromatic images (VMIs).

Since the use of iodine-based contrast agents is essential for effective clinical diagnosis, the ability to generate VUE images offers the potential for significant radiation dose reduction. Previous workers found that the generation of VMI at approximately 70 keV yielded optimal levels of image noise and contrast-to-noise ratio (CNR) for identification of hepatic lesions [3]. VMIs also show reduced beam-hardening artifacts and more quantitatively accurate measurements of X-ray attenuation [4]. Therefore, in this study, VUE images under different IFRs were generated based on monochromatic images of 70 keV. In recent work, Zhang et al. [5] found that the attenuation values from the aorta differed significantly between TUE and VUE images. Similarly, Barrett et al. [6] found differences between attenuation values on VUE and unenhanced images of the liver. The reasons for these observed differences are likely to be multifactorial; however, the finding of changes in the aorta raises the possibility that they reflect variations in performance of the analysis algorithm in the presence of high contrast agent concentrations.

The purpose of this study is to evaluate whether variation in iodine flow rates (IFRs) and iodine concentration in different groups, consequently in peak vascular iodine concentrations, affects the quality or diagnostic utility of VUE images in abdominal multiphasic CT.

Methods

Patients

This prospective study was approved by the Institutional Review Board, and each participant provided written informed consent. One hundred and four patients were recruited between December 2013 and June 2014 and randomized to one of 4 groups with different IFRs and contrast agent concentrations (A–D; Table 1), with 26 patients in each group. Among those patients, ten were excluded due to artifacts or poor image quality, and the other ninety-four patients were included. The flow rates ranged from 3 to 5 ml/s (as commonly used in clinical) with a fixed injection time of 20 s. (1) Patients who provided written informed consent; (2) patients who breathe naturally and calmly; and (3) patients referred for unenhanced and triphasic contrast-enhanced CT scan of the abdomen (range from diaphragm to pubic symphysis) were included in this study. Exclusion criteria were (1) written informed consent not available; (2) risk of pregnancy; (3) contraindications to iodinated contrast material, such as previous history of anaphylactic reaction; (4) artifacts or poor image quality.

Scanning Protocol

All CT examinations were performed with a dual-energy Gemstone Spectral CT (Discovery CT750HD scanner, GE Healthcare, Waukesha, WI, USA). An initial unenhanced scan was performed for all patients in the supine position, from the dome of the liver to the iliac crest within one breathhold. It was followed by a triphasic contrast-enhanced acquisition with dual-energy mode. The unenhanced scan was acquired with tube voltage of 120 kVp and automatic tube current (290–650 mA). The triphasic contrast-enhanced scanning was acquired in dual-energy mode with fast kVp-switching between 80 and 140kVp, automatic tube current modulation, 0.984 pitch, 5 mm slice thickness, 0.5 s rotation time, and an FOV of 38 × 38 mm. Contrast agent under different IFRs was administered by a power injector (Empower CTA, ACIST, USA) through a cannula in an antecubital vein, using one of the four injection protocols shown in Table 1, and was followed by a 20 ml saline flush at the same injection rate. The timing of the arterial enhancement phase was selected using SmartPrep technology, with the ROI for the trigger pulse placed at the root of abdominal aorta and a triggering threshold of 100 HU at 80 kVp [7]. The images of the arterial phase were acquired at 10 s after triggering. The portal venous phase collection commenced 30 s after the arterial phase and the delayed phase 90 s after the arterial phase.

Table 1. Injection protocols of different groups (with a fixed injection time of 20 s)

Group	n	Contrast agent and concentration (mg I/ml)	Flow rate (ml/s)	IFR (g I/s)	Total iodine (g)
A	24	Iohexol 350	4.0	1.4	28
B	22	Iohexol 350	3.43	1.2	24
C	26	Iodixanol 320	4.375	1.4	28
D	22	Iodixanol 320	3.75	1.2	24

Table 2. Grading scale for subjective quality

	Image quality		
Grading scale	Noise	Artifacts	Anatomical details and lesions
5	Minimum or no image noise	No or minimal artifacts	Clearly
4	Less than average noise	Artifacts occupying a part of the body, but not interfering with diagnostic decision making	Clearly
3	Average image noise	Noise and artifacts are obvious but acceptable	Owed clear anatomical detail, lesions appeared well
2	Above average noise	Artifacts affecting diagnostic information	Identification of anatomical details was difficult, lesions shown were not clear
1	Unacceptable image noise	Not applicable	Unable to identify anatomical detail and lesions

Table 3. Patient characteristics of different groups

Group	Weight (kg)	Height (m)	BMI (kg/m^2)	Age (years)	Gender (M/F)*
Group A	68.09 ± 8.04	1.69 ± 0.08	24.23 ± 2.19	54.21 ± 9.86	18/6
Group B	64.11 ± 11.37	1.63 ± 0.09	23.52 ± 3.50	54.05 ± 12.12	17/5
Group C	64.83 ± 7.51	1.67 ± 0.08	23.13 ± 1.82	53.81 ± 6.98	19/7
Group D	66.21 ± 10.23	1.68 ± 0.08	23.35 ± 2.55	54.41 ± 8.66	18/4
p	0.296	0.073	0.334	0.997	0.907

* χ^2 tests

Image reconstruction

All images were reconstructed with 40% adaptive statistical reconstruction (AsiR) techniques [8]. VUE images under different IFRs were generated based on monochromatic images of 70 keV using a standard, two-material decomposition algorithm [8], using Advantage Workstation (GE AW 4.6). The study dataset therefore consisted of 4 separate patient groups defined by injection protocol (Table 1) and 4 comparable phase images (unenhanced, arterial phase, venous phase, delayed phase) for each patient.

Image evaluation

Objective image quality assessment

Objective image quality assessment was performed on all datasets. Image noise, SNR, and CNR were assessed by placement of three regions of interest in each of the following: (1) abdominal aorta, (2) liver (right lobe, near the edge to avoid vascular area), (3) spleen (near the edge to avoid vascular area), (4) retroperitoneal fat, (5) erector spinae of both sides (at the level of the origin of the superior mesenteric artery), (6) portal vein (at the bifurcation of left and right portal veins), (7) pancreatic head, and (8) each hepatic lesion (at the level of maximum size). The size and shape of the ROIs were maintained the same, at approximately 1 cm^2, by use of the copy-and-paste function. Then the mean values were recorded. All datasets were randomized to enable double-blind evaluation with all patient information removed. The mean CT attenuation values (HU) and objective image noise (standard deviation of the CT numbers) were recorded for all ROIs of all image sets.

Signal-to-noise ratio (SNR) was calculated by dividing the mean HU values by the corresponding image noise. The CNRs were calculated as follows [9, 10]:

$$CNR = \left(ROI_{target} - ROI_{Background}\right) / SD_{Background},$$

where ROI_{target} denotes the mean HU values of the target ROI, $ROI_{Background}$ denotes the mean HU of fat, and $SD_{Background}$ denotes the standard deviation of the distribution of HU from fat. The same background was used for all target ROIs in calculating CNR.

Subjective image quality assessment

The subjective image quality was independently assessed by two radiologists (9 and 17 years of experience) each blinded to the scoring of the other. Images were evaluated using a fixed abdominal window setting (window width, 400 HU; window level, 40HU). Subjective image quality was assessed on a 5-point scale with 3 separate components reflecting the (1) clarity of demonstration of lesions and anatomical structures, (2) severity of imaging artifacts, and (3) severity of background noise (Table 2). The scores from the three domains were then averaged to give an overall score for image quality).

The consistency of the analysis results of two radiologists was checked. The averages of the two individual radiologists' scores were used for image quality evaluation. A subjective image quality score ≥3 was considered to represent images of diagnostic quality.

Radiation dosage assessment

For each patient in different groups, the dose–length product (DLP) was recorded from the dose report for the entire examination. The effective dose (ED) estimate was

determined from DLP measurements and appropriate normalized coefficients for abdominal CT (0.015 mSv/ (mGy*cm)) [11]. Mean values of DLP and ED for an examination with and without a plain scan phase were calculated in order to assess the potential percentage dose savings.

Statistical analysis

All data were analyzed using SPSS (Version 22; IBM, New York, USA). The Kolmogorov–Smirnov test was used first to test for normal distribution. Where data conformed to a normal distribution, analysis of variance was used to compare the mean HU values, image noise, SNRs, and CNRs for the 4 image sets. Where data distribution was not normal, a nonparametric test (Kruskal–Wallis test followed by stepwise step-down comparisons) was used. The significance level for all tests was 0.01 (two-sided) to allow for type 2 errors due to multiple testing.

The consistency of the analysis results of two radiologists was checked using Kappa-test.

Results

Patients

A total of 94 patients were recruited in four different groups within the study period. Complete datasets were acquired from all patients and all were included in the analysis. Patient demographic characteristics (Table 3) showed no significant differences between the groups A–D.

Image quality assessment

The mean HU values on all target ROIs in different groups (Table 4) showed no significant differences between the 4 patient groups under different IFRs or between image types in the same group under the same IFR ($p > 0.01$). Comparison of objective image noise

Table 4. Comparison of CT values (in HU) between VUE and TUE images in the same group and between groups (A–D)

Position	Phase	A	B	C	D	p
Aorta	TUE	46.29 ± 6.48	48.25 ± 6.08	48.70 ± 4.16	47.75 ± 6.22	0.718*
	VUE-AP	47.00 ± 7.86	50.72 ± 6.74	50.15 ± 10.22	51.01 ± 5.96	0.069*
	VUE-VP	46.83 ± 7.64	50.01 ± 4.94	50.82 ± 4.41	47.62 ± 4.84	0.077*
	VUE-DP	44.81 ± 7.98	47.32 ± 4.86	49.33 ± 3.52	46.03 ± 5.17	0.076*
p		0.547*	0.184	0.036*	0.031	–
Portal	TUE	42.18 ± 6.71	43.58 ± 6.72	45.54 ± 4.41	45.68 ± 5.25	0.122
	VUE-AP	43.64 ± 7.58	46.38 ± 5.01	48.03 ± 4.36	46.74 ± 4.92	0.053
	VUE-VP	45.97 ± 7.55	46.62 ± 5.71	47.85 ± 4.86	49.18 ± 6.02	0.438*
	VUE-DP	44.77 ± 8.20	44.72 ± 5.84	47.03 ± 4.83	45.50 ± 5.41	0.593*
p		0.088*	0.270	0.202	0.100	–
Liver	TUE	63.65 ± 7.27	63.82 ± 8.07	66.34 ± 5.45	65.25 ± 8.41	0.678*
	VUE-AP	60.62 ± 6.92	63.08 ± 7.11	64.85 ± 5.29	62.72 ± 7.19	0.204*
	VUE-VP	61.90 ± 7.76	64.53 ± 8.78	65.81 ± 5.55	64.76 ± 6.09	0.267
	VUE-DP	60.89 ± 8.29	64.31 ± 8.11	65.05 ± 5.36	64.32 ± 7.31	0.187*
p		0.504	0.525*	0.734	0.685	
Lesion of liver	TUE	35.78 ± 13.39	44.57 ± 12.75	36.10 ± 15.84	42.92 ± 14.80	0.297
	VUE-AP	35.53 ± 13.51	44.42 ± 14.47	36.24 ± 15.55	42.06 ± 12.27	0.331
	VUE-VP	36.10 ± 13.41	42.98 ± 14.23	34.89 ± 14.89	43.08 ± 15.07	0.352*
	VUE-DP	37.06 ± 15.01	42.88 ± 12.75	32.62 ± 14.11	42.98 ± 15.65	0.352*
p		0.989	0.985	0.684*	0.997	–
Pancreas	TUE	47.58 ± 8.87	50.10 ± 6.75	48.91 ± 6.85	50.29 ± 5.04	0.534
	VUE-AP	47.92 ± 9.92	49.73 ± 5.19	50.24 ± 6.42	51.81 ± 4.34	0.295
	VUE-VP	47.40 ± 9.99	50.05 ± 4.88	49.47 ± 7.13	50.95 ± 5.61	0.394
	VUE-DP	46.76 ± 9.72	49.93 ± 5.53	48.85 ± 5.88	49.62 ± 5.40	0.400
p		0.980	0.997	0.862	0.533	–
Spleen	TUE	62.81 ± 7.43	62.86 ± 6.68	62.32 ± 4.69	64.05 ± 5.52	0.541*
	VUE-AP	60.88 ± 8,.16	62.24 ± 5.78	62.34 ± 5.53	62.85 ± 4.55	0.964*
	VUE-VP	60.28 ± 8.09	63.65 ± 5.90	62.48 ± 5.27	63.24 ± 5.17	0.550*
	VUE-DP	59.73 ± 7.84	60.03 ± 5.11	60.28 ± 5.38	62.03 ± 4.01	0.586*
p		0.314*	0.820	0.416	0.579	–
Retroperitoneal fat	TUE	−85.08 ± 13.69	−83.45 ± 17.61	−85.47 ± 10.94	−83.80 ± 11.32	0.948*
	VUE-AP	−83.59 ± 14.59	−83.91 ± 18.67	−84.39 ± 10.30	−80.60 ± 12.55	0.755*
	VUE-VP	−79.76 ± 16.02	−80.62 ± 16.06	−81.73 ± 11.68	−76.81 ± 12.14	0.544*
	VUE-DP	−79.74 ± 14.91	−78.46 ± 15.41	−80.17 ± 12.11	−76.18 ± 12.01	0.684*
p		0.494	0.580*	0.203*	0.132	–
Erector Spinae	TUE	63.98 ± 12.23	64.09 ± 4.91	65.65 ± 6.86	65.43 ± 6.95	0.668*
	VUE-AP	60.23 ± 11.75	61.37 ± 4.86	62.06 ± 6.62	61.19 ± 4.77	0.971*
	VUE-VP	61.22 ± 10.73	62.27 ± 5.12	62.50 ± 6.55	63.23 ± 4.12	0.931*
	VUE-DP	60.90 ± 10.88	61.60 ± 4.21	62.44 ± 5.68	62.44 ± 5.07	0.977*
p		0.112*	0.233	0.183*	0.069	–

The significance level for all tests was 0.01 (two-sided) to allow for type 2 errors due to multiple testing
TUE true unenhanced, *VUE-AP* VUE images of arterial phase, *VUE-VP* VUE images of portal phase, *VUE-DP* VUE images of delayed phase
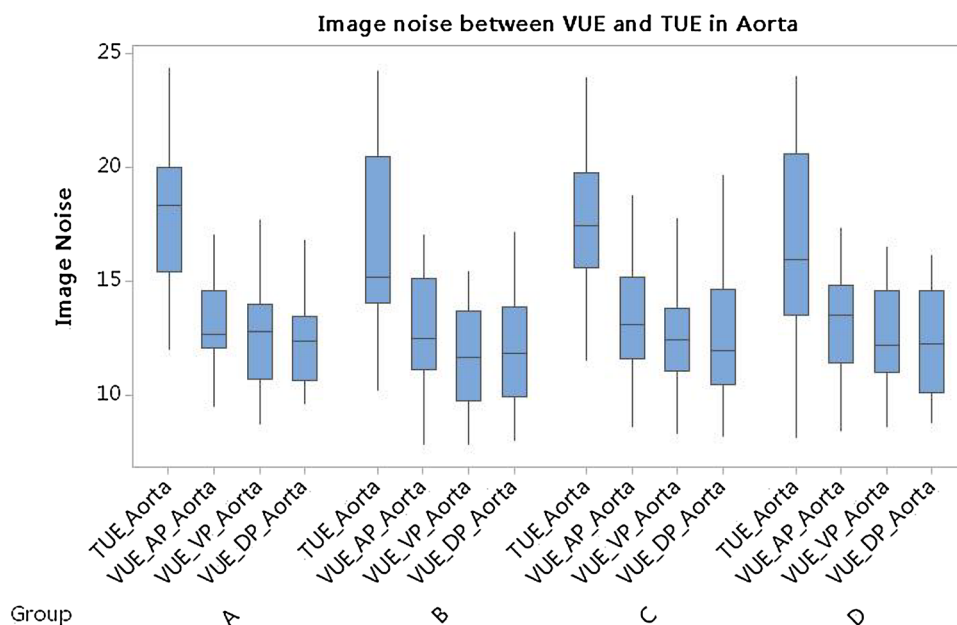* Nonparametric test

Fig. 1. Comparison of image noise between VUE and TUE images in aorta. There were no statistical differences for the same image type between the 4 patient groups ($p > 0.05$), but significant differences between different image types within groups ($p = 0.000$).
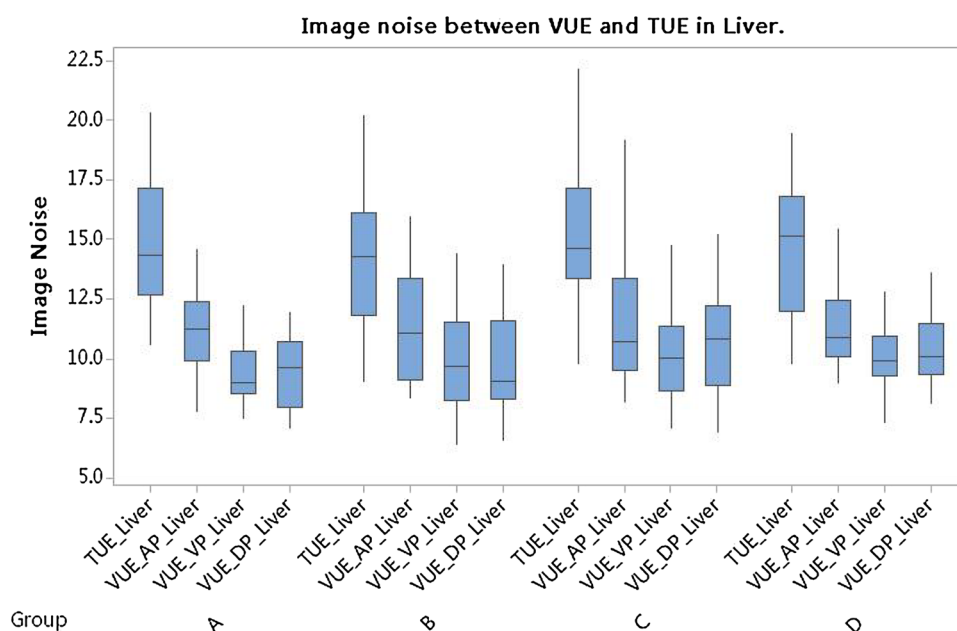

Fig. 2. Comparison of image noise between VUE and TUE images in liver parenchyma. There were no statistical differences for the same image type between the 4 patient groups ($p > 0.05$), but significant differences between different image types within groups ($p = 0.000$).

between VUE images under different IFRs and unenhanced images showed noise values to be similar or significantly lower in VUE images, as shown in aorta (Fig. 1) or liver (Fig. 2). Comparison of SNR and CNR values (Figs. 3, 4) reflected that equivalent or significantly higher image quality was presented in VUE images compared to unenhanced CT (Table 5).

The Kappa value of the analysis results of two radiologists was $K = 0.589$, $p < 0.001$. Subjective analysis of image quality showed that the quality of VUE images under different IFRs was equivalent or slightly lower ($p > 0.05$) than that of unenhanced CT but all were of acceptable diagnostic quality (Table 6; Figs. 5, 6).

Radiation dose

The mean radiation dose savings, resulting from the use of VUE images, are shown in Tables 7 and 8. Removing unenhanced images from the protocol used in the present cohort of patients would have resulted in a theoretical dose saving of approximately 25% in both DLP and ED.

Discussion

This prospective study showed that VUE images can eliminate the need for unenhanced abdominal CT images over a range of iodine flow rates (IFRs) and iodine
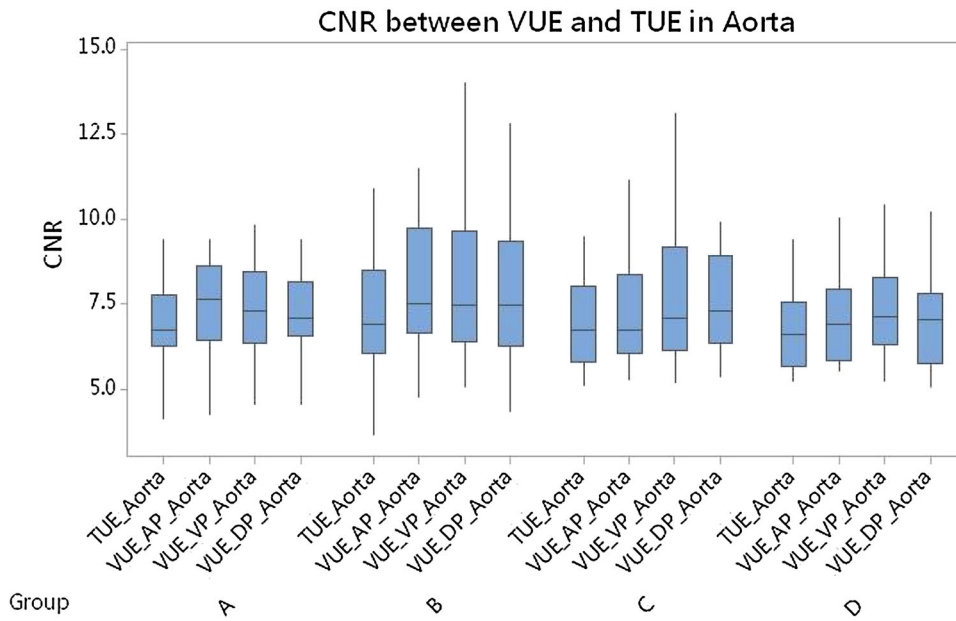
Fig. 3. Comparison of CNR between VUE and TUE images in aorta. There were no significant differences between the 4 patient groups or between image types within the same group ($p > 0.05$).
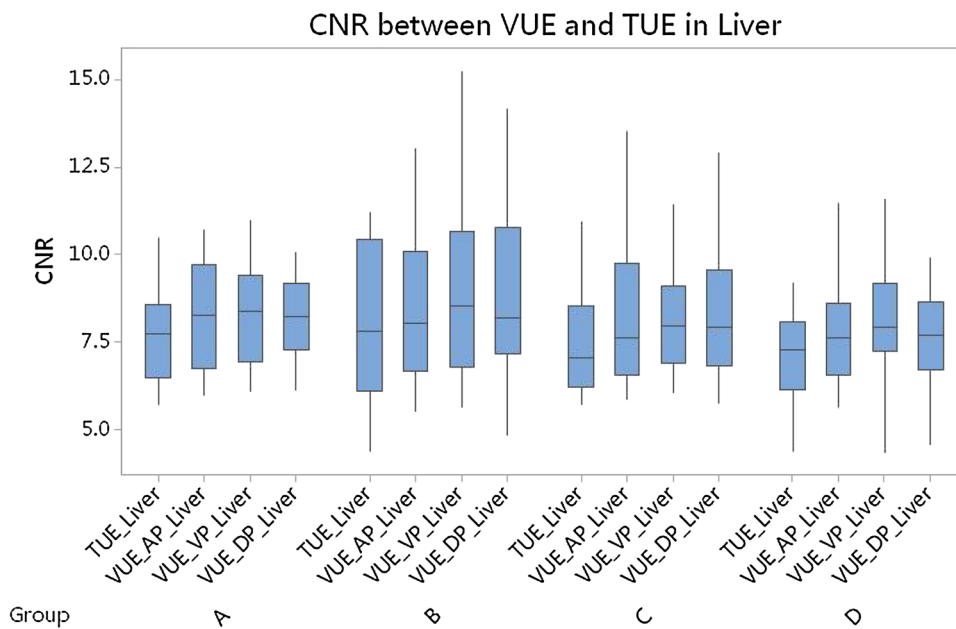

Fig. 4. Comparison of CNR between VUE and TUE images in liver parenchyma. There were no significant differences between different groups or between image types within the same group ($p > 0.05$).

concentrations in different groups with significant reduction in radiation dose. The subjective image quality of VUE images was comparable to unenhanced CT, and SNR as well as CNR was equivalent or improved.

The finding of the improved SNR and CNR characteristics seems initially counterintuitive but has also been reported by previous workers [1, 2]. It is believed to represent a combination of image smoothing, imposed by the post-processing algorithm, and a genuine increase in tissue/background ratio on synthesized monochromatic images. This study together with the findings of previous workers demonstrates no disadvantages associated with the use of VUE in place of unenhanced CT

images. The use of such an abbreviated imaging protocol in the current series would result in a dose reduction in the region of 25%, similar to previous studies which described potential dose reductions of 24.8–35.1% [1, 2, 4].

The major motivation of the current study was to ensure that clinically acceptable variations in the rate of iodine administration, and consequently in the peak vascular iodine concentration, do not adversely affect the quality of VUE images. No previous clinical studies have addressed this aspect of monochromatic VUE generation. In principle, the difference in X-ray attenuation between soft tissues and iodine reflects two components. Firstly, there is a very significant difference in the energy

Table 5. Comparison of SNR between VUE and TUE images within groups and between groups (A–D)

Position	Phase	A	B	C	D
Aorta	TUE	2.70 ± 0.70	3.13 ± 0.95	2.86 ± 0.67	3.07 ± 0.98
	VUE-AP	3.62 ± 1.02	4.17 ± 1.12	3.93 ± 1.16	3.97 ± 1.99
	VUE-VP	3.80 ± 0.99	4.53 ± 1.03	4.22 ± 0.98	3.92 ± 0.80
	VUE-DP	3.70 ± 0.94	4.19 ± 1.13	4.14 ± 0.87	3.91 ± 0.96
p		0.000	0.000	0.000	0.005
Average growth (%)		37.28	37.27	43.24	28.12
Portal	TUE	2.56 ± 0.68	3.08 ± 1.06	2.82 ± 0.67	2.98 ± 0.82
	VUE-AP	3.04 ± 0.66	3.70 ± 0.89	3.42 ± 0.87	3.28 ± 0.69
	VUE-VP	3.72 ± 0.96	4.01 ± 0.77	4.22 ± 1.17	3.98 ± 0.91
	VUE-DP	3.82 ± 1.11	3.96 ± 1.30	3.78 ± 1.06	3.81 ± 0.98
p		0.000	0.010	0.000	0.001
Average growth(%)		37.76	26.30	34.99	23.83
Liver	TUE	4.51 ± 1.07	4.64 ± 1.29	4.59 ± 1.02	4.58 ± 1.19
	VUE-AP	5.61 ± 1.25	5.85 ± 1.56	5.85 ± 1.53	5.69 ± 1.19
	VUE-VP	6.73 ± 1.73	6.87 ± 2.09	6.59 ± 1.21	6.54 ± 1.31
	VUE-DP	6.61 ± 1.39	6.84 ± 1.99	6.22 ± 1.52	6.33 ± 1.37
p		0.000	0.000	0.000	0.000
Average growth (%)		40.06	40.52	35.51	35.08
Lesion of liver	TUE	2.53 ± 1.20	3.24 ± 1.37	2.62 ± 1.20	2.82 ± 1.07
	VUE-AP	2.85 ± 1.10	4.07 ± 1.86	3.24 ± 1.90	3.15 ± 1.62
	VUE-VP	3.42 ± 1.50	4.86 ± 2.62	2.90 ± 1.39	3.46 ± 1.68
	VUE-DP	3.66 ± 1.98	4.04 ± 1.97	2.68 ± 1.35	3.33 ± 1.83
p		0.113	0.674	0.904	0.198
Average growth (%)		30.83	33.44	12.21	17.61
Pancreas	TUE	2.94 ± 0.93	3.26 ± 0.94	3.07 ± 0.72	3.10 ± 0.86
	VUE-AP	3.74 ± 1.04	4.05 ± 1.06	4.00 ± 1.07	3.97 ± 0.90
	VUE-VP	4.02 ± 1.25	4.37 ± 1.03	4.36 ± 1.37	4.31 ± 1.05
	VUE-DP	4.05 ± 1.32	4.39 ± 1.28	4.18 ± 1.02	4.31 ± 0.96
p		0.003	0.003	0.000	0.000
Average growth (%)		33.90	30.98	36.16	35.38
Spleen	TUE	3.65 ± 1.01	4.36 ± 1.32	3.75 ± 0.77	4.12 ± 1.21
	VUE-AP	5.03 ± 1.04	5.65 ± 1.04	4.76 ± 1.03	5.33 ± 1.29
	VUE-VP	5.69 ± 1.17	6.53 ± 1.17	5.65 ± 1.14	5.91 ± 1.19
	VUE-DP	5.35 ± 1.12	6.15 ± 1.28	5.49 ± 1.04	5.71 ± 1.34
p		0.000	0.000	0.000	0.000
Average growth (%)		40.76	40.14	41.33	37.14
Erector spinae	TUE	3.65 ± 1.05	3.88 ± 1.17	3.77 ± 1.60	3.87 ± 0.97
	VUE-AP	4.40 ± 1.28	4.88 ± 1.37	4.62 ± 1.31	4.29 ± 0.96
	VUE-VP	5.11 ± 1.11	5.44 ± 1.73	5.05 ± 1.37	4.95 ± 0.97
	VUE-DP	5.38 ± 1.93	5.52 ± 1.60	5.11 ± 1.38	4.87 ± 0.95
p		0.000	0.001	0.000	0.001
Average growth (%)		35.98	36.08	30.68	21.53

The average percentage increase of SNR from unenhanced to the 3 enhanced phases was marked as Average growth (%)

Table 6. Mean subjective scores of the 4 phases in different groups

Group	TUE	VUE-AP	VUE-VP	VUE-DP
A	5	4.67 ± 0.76	4.63 ± 0.88	4.38 ± 1.06
B	5	4.86 ± 0.35	4.82 ± 0.50	4.82 ± 0.50
C	5	4.81 ± 0.60	4.73 ± 0.81	4.73 ± 0.81
D	5	4.77 ± 0.61	4.73 ± 0.77	4.68 ± 0.89

dependence of X-ray attenuation between soft tissues, bone, and iodine. Secondly, iodine exhibits a prominent K-edge absorption peak at 33.2 keV. A number of post acquisition algorithmic approaches exist to support the generation of virtual monochromatic images from this kind of data. Although simple linear optimization approaches have proven relatively effective [12], attempts to minimize estimation errors have led to the widespread use of iterative maximum likelihood (ML) algorithms. Using ML decomposition, estimated errors on monochromatic image generation are reduced to below 5% [13]. Previous workers found that the generation of virtual monochromatic image at approximately 70 keV yielded optimal levels of image noise and contrast-to-noise ratio (CNR) for identification of hepatic lesions [3]. VMIs also show reduced beam-hardening artifacts and more quantitatively accurate measurements of X-ray attenuation [4]. Therefore, in our study, VUE images under different
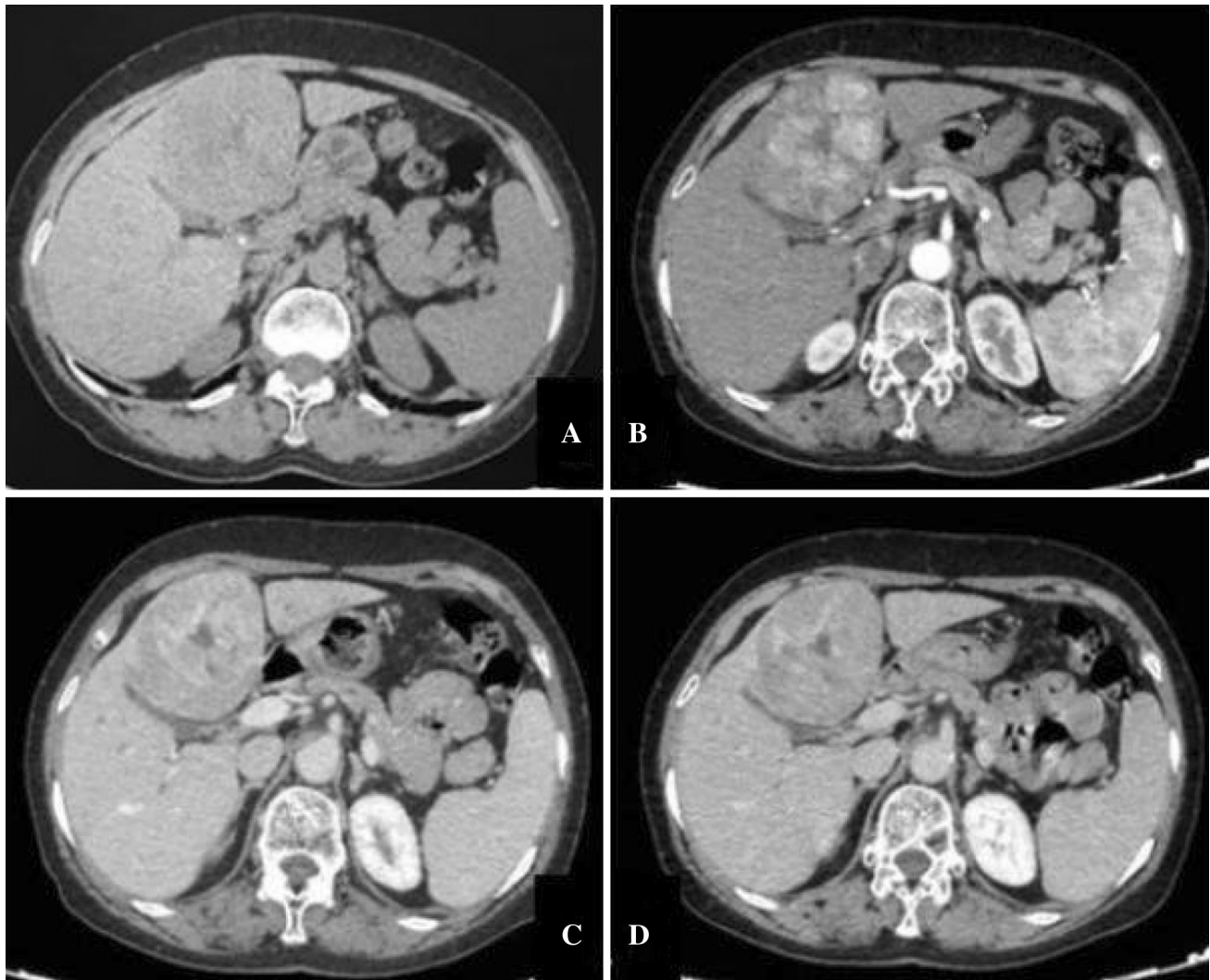
Fig. 5. A 55-year-old male patient in Group B diagnosed with hepatocellular carcinoma in the left lobe of liver: (**A**) unenhanced, (**B**) arterial phase, (**C**) portal phase, and (**D**) delayed phase. Tumor showed hyperintense enhancement in the arterial phase and hypointense enhancement in the portal and delayed phases.

IFRs were generated based on monochromatic images of 70 keV. In this study, we found that variation in iodine flow rates (IFR) and consequently in peak vascular iodine concentrations does not affect the quality or diagnostic utility of VUE images in abdominal multiphasic CT which can potentially reduce the amount of contrast agent we use in clinical diagnosis.

Several groups have previously evaluated the quality of VUE images. Yamada et al. [14] showed that VUE images generated as monochromatic images at 70 keV provided reduced objective image noise, increased SNR and CNR, and a better subjective image quality while maintaining image sharpness when compared with conventional unenhanced polychromatic images. In an earlier study, Yamada et al. [15] showed that the use of VUE images allows the calculation of dose distribution in radiotherapy treatment planning which entirely com-

pensates for the presence of iodine in contrast-enhanced images. Graser et al. [16] found no statistical difference in attenuation values in the liver, renal parenchyma, aorta, and psoas muscles using VUE images derived from the nephrographic phase of enhancement. Besides, Chai et al. [17] showed that in patients with gastric tumors, the VUE images derived from single-source fast kVp-switching dual-energy CT can provide comparable image quality to TUE images and reliable diagnostic information, and replacing TUE images will lower radiation dose by 30.5%. Zhang et al. [5] also found that attenuation values on VUE images derived from the arterial and portal venous phases were similar to those on unenhanced images on liver, spleen, and pancreas. However, attenuation values from the aorta and fat were significantly different. Recently, Barrett et al. [6] found significant differences between attenuation values from
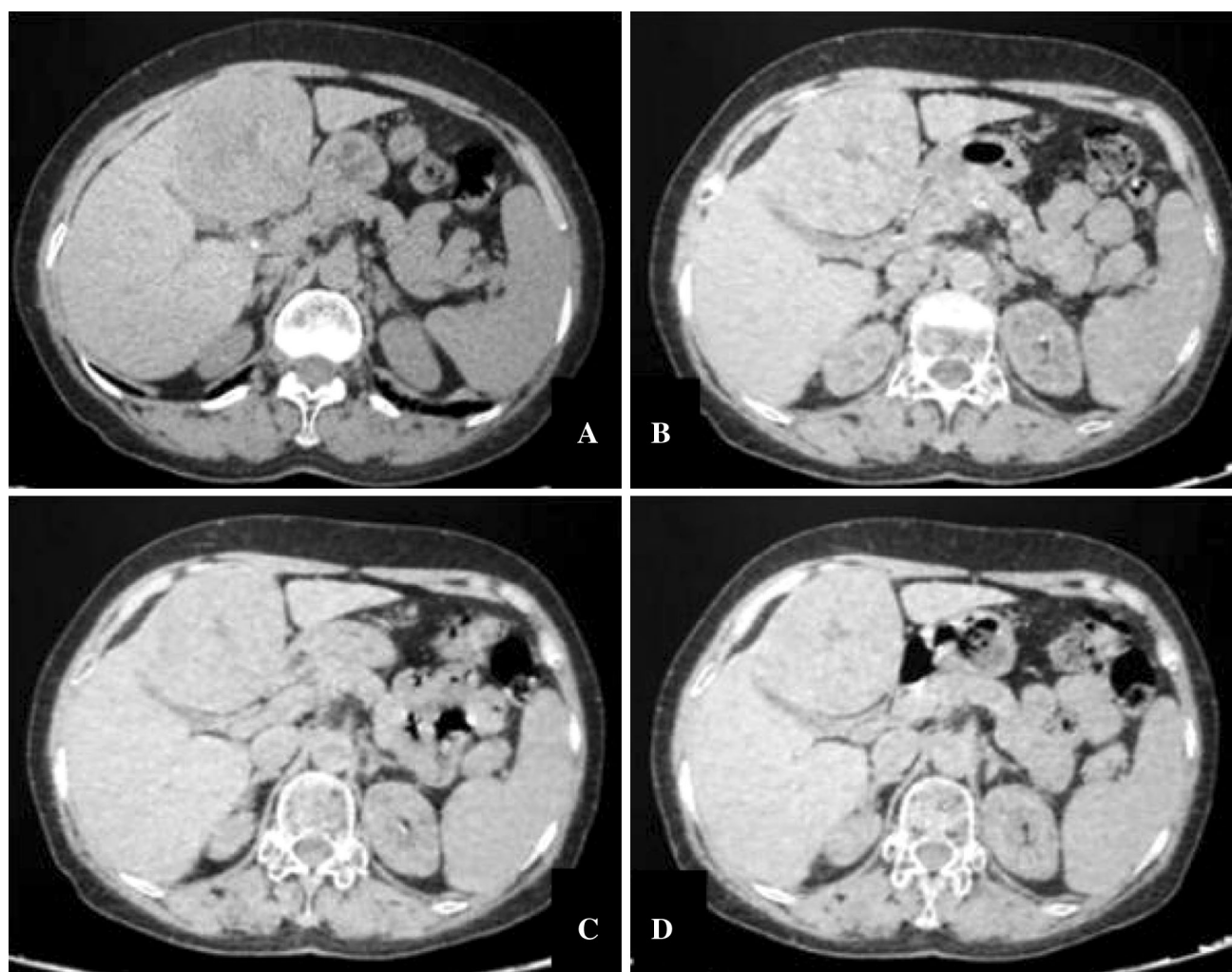
Fig. 6. TUE and VUE images of the same patient in Fig. 5: (**A**) unenhanced, (**B**) VUE images of arterial phase, (**C**) VUE images of the portal phase, and (**D**) VUE images of the delayed phase. The VUE images were of acceptable diagnostic quality. The central scar in the lesion showed better contrast (CNR_{AP} = 11.88, CNR_{VP} = 12.28, CNR_{DP} = 11.61) in VUE images than unenhanced image (CNR_{CU} = 10.65), where CNR_{CU}, CNR_{AP}, CNR_{VP}, and CNR_{DP} are CNR values of the unenhanced, arterial phase, portal phase and delayed phase, respectively.

VUE and unenhanced images of liver in arterial and portal venous phases. The reasons for observed differences in attenuation values between unenhanced and VUE images are multifactorial [18]. Factors that have been postulated to cause unreliable iodine subtraction include large patient population, areas of beam-hardening artifact, and very high iodine concentrations. Furthermore, certain parameters in the post-processing software are preset by the user, including attenuation values for soft tissue and fat. Incorrect parameter values will result in inaccurate iodine subtraction. Miller et al. [19] recently investigated the effect of body habitus and individual organ enhancement on the iodine subtraction algorithm. By correcting for body habitus and individual organ enhancement, they demonstrated no significant differences in attenuation values in the liver, spleen, pancreas, kidneys, and aortic blood pool between TUE and VUE images. But yet only few studies have investigated whether variation in IFR and consequently in peak vascular iodine concentrations affects the quality or diagnostic utility of VUE images in abdominal multiphasic CT. In this study, we found no differences between aorta, portal vein, liver, liver lesion, pancreas, spleen, erector spinae, and retroperitoneal fat under different iodine flow rates and contrast agent concentrations.

The limitation of our study is that not all the iodine flow rates used in clinical diagnosis were tested due to the limited number of patients recruited. In statistical analysis, comparing intra-subject attenuation changes between VUE and TUE images may reveal more information than using mean attenuation. And most

Table 7. Dose–length product (DLP) (mGy-cm) in different groups

DLP (Gmy)	TUE	VUE-AP	VUE-VP	VUE-DP	Total
A	524.79 ± 47.14	537.062 ± 50.85	537.062 ± 50.86	537.0618 ± 50.85	2145.187 ± 191.53
B	533.78 ± 45.80	544.016 ± 47.43	544.016 ± 47.43	544.0164 ± 47.43	2187.384 ± 184.37
C	499.9 ± 31.56	503.872 ± 31.95	503.872 ± 31.95	503.8724 ± 31.95	2031.533 ± 120.19
D	543.66 ± 48.32	544.217 ± 41.76	544.217 ± 41.76	544.2173 ± 41.76	2203.559 ± 173.79

Table 8. Average effective radiation dose (ED = DLP × 0.015) in different groups

ED (mGy-cm)	TUE	VUE-AP	VUE-VP	VUE-DP	Total	%
A	7.87 ± 0.71	8.06 ± 0.76	8.06 ± 0.76	8.06 ± 0.76	32.18 ± 2.87	24.46
B	8.01 ± 0.69	8.16 ± 0.71	8.16 ± 0.71	8.16 ± 0.71	32.81 ± 2.77	24.41
C	7.50 ± 0.47	7.56 ± 0.48	7.56 ± 0.48	7.56 ± 0.48	30.47 ± 1.80	24.61
D	8.15 ± 0.72	8.16 ± 0.63	8.16 ± 0.63	8.16 ± 0.63	33.05 ± 2.61	24.66

patients had a BMI < 28, and further study on patients with larger BMI will be performed.

Conclusion

VUE images from dual-energy multiphasic liver CT scans have the potential to replace conventional unenhanced images. Measured tissue and vascular attenuation values on VUE images are not significantly different from unenhanced CT images and this is true over the entire range of iodine concentrations likely to be observed in clinical practice. Clinically, diagnostic multiphase CT examinations of the liver could be achieved with a potential saving in the radiation dose of 25%.

References

1. Sakane M, Kim T, Hori M, et al. (2014) Effects of High-concentration contrast material and low-voltage CT on contrast for multiphasic CT of the upper abdomen: comparison using the simulation with virtual monochromatic imaging obtained by fast-switch kVp dual-energy CT. SpringerPlus 3:234
2. Matsumoto K, Jinzaki M, Tanami Y, et al. (2011) virtual monochromatic spectral imaging with fast kilovoltage switching: improved image quality as compared with that obtained with conventional 120-kVp CT. Radiology 259:257–262
3. Yamada Y, Jinzaki M, Tanami Y, et al. (2012) Virtual monochromatic spectral imaging for the evaluation of hypovascular hepatic metastases: the optimal monochromatic level with fast kilovoltage switching dual-energy computed tomography. Investig Radiol 47:292–298
4. Goodsitt MM, Christodoulou EG, Larson SC (2011) Accuracies of the synthesized monochromatic CT numbers and effective atomic numbers obtained with a rapid kVp switching dual energy CT scanner. Med Phys 38:2222–2232
5. Zhang L-J, Peng J, Wu S-Y, et al. (2010) Liver virtual non-enhanced CT with dual-source, dual-energy CT: a preliminary study. Eur Radiol 20:2257–2264
6. Barrett T, Bowden DJ, Shaida N, et al. (2012) Virtual unenhanced second generation dual-source CT of the liver: Is it time to discard the conventional unenhanced phase? Eur J Radiol 81:1438–1445
7. Yu L, Leng S, McCollough CH (2012) Dual-energy CT-based monochromatic imaging. AJR AmJ Roentgenol 199:S9–S15
8. Cornfeld D, Israel G, Detroy E, et al. (2011) Impact of Adaptive Statistical Iterative Reconstruction (ASIR) on radiation dose and image quality in aortic dissection studies: a qualitative and quantitative analysis. AJR Am J Roentgenol 196:W336–W340
9. Kalra MK, Maher MM, Sahani DV, et al. (2003) Low-dose CT of the abdomen: evaluation of image improvement with use of noise reduction filters—pilot study. Radiology 228:251–256
10. Pinho DF, Kulkarni NM, Krishnaraj A, et al. (2012) Initial experience with single-source dual-energy CT abdominal angiography and comparison with single-energy CT angiography: image quality, enhancement, diagnosis and radiation dose. Eur Radiol 23:351–359
11. American Association of Physicists in Medicine. The measurement, reporting, and management of radiation dose in CT; January 2008. http://www.aapm.org/pubs/reports/rpt_96pdf. Accessed 15 Feb 2014
12. Alvarez RE, Seppi EA (1979) Comparison of noise and dose in conventional and energy selective computed tomography. IEEE Trans Nucl Sci 26:2853–2856
13. Bornefalk H, Persson M (2014) Theoretical comparison of the iodine quantification accuracy of two spectral CT technologies. IEEE Trans Med Imaging 33:556–565
14. Yamada Y, Jinzaki M, Hosokawa T, et al. (2014) Abdominal CT: an intra-individual comparison between virtual monochromatic spectral and polychromatic 120-kVp images obtained during the same examination. Eur J Radiol 83:1715–1722
15. Yamada S, Ueguchi T, Ogata T, et al. (2014) Radiotherapy treatment planning with contrast-enhanced computed tomography: feasibility of dual-energy virtual unenhanced imaging for improved dose calculations. Radiat Oncol 9:168
16. Graser A, Johnson TRC, Hecht EM, et al. (2009) Dual-energy CT in patients suspected of having renal masses: can virtual nonenhanced images replace true nonenhanced images? Radiology 252:433–440
17. Chai Y, Xing J, Gao J, et al. (2016) Feasibility of virtual nonenhanced images derived from single-source fast kVp-switching dual-energy CT in evaluating gastric tumors. Eur J Radiol 85:366–372
18. Sahni VA, Shinagare AB, Silverman SG (2013) Virtual unenhanced CT images acquired from dual-energy CT urography: accuracy of attenuation values and variation with contrast material phase. Clin Radiol 68:264–271
19. Miller CM, Gupta RT, Paulson EK, et al. (2011) Effect of organ enhancement and habitus on estimation of unenhanced attenuation at contrast-enhanced dual-energy MDCT: concepts for individualized and organ-specific spectral iodine subtraction strategies. AJR Am J Roentgenol 196:W558–W564